

Aerothermal analysis of the RETALT2 vehicle

Mariasole Laureti[†] and Sebastian Karl
DLR Institute of Aerodynamics and Flow Technology - Spacecraft
Bunsenstr. 10, 37073 Göttingen, Germany
mariasole.laureti@dlr.de · sebastian.karl@dlr.de
[†]Corresponding author

Abstract

In the framework of the Horizon 2020 project RETALT (Retro Propulsion Assisted Landing Technologies), whose main objective was the investigation of technologies for reusable launch systems, a Single Stage To Orbit (SSTO) Vertical Take-off Vertical Landing (VTVL) launcher configuration, called RETALT2, was studied. This paper aims at describing the generation of Aero-Thermal Databases (ATDBs) for surface heat fluxes as fast-response surrogate models for the aero-thermodynamic heating of the vehicle surface over the entire trajectory, i.e. ascent and re-entry. Representative flow field solutions are discussed in terms of flow field topology and resulting heat patterns on the vehicle surface. Furthermore, the time evolution over the entire flight path of area-averaged heat fluxes on the vehicle nose and base plate are shown and analysed.

Acronyms & Symbols

ACS	= Aerodynamic Control Surfaces	M	= Mach number
ATDB	= Aero-Thermal Data Base	q	= Heat flux per unit area (kW/m^2)
CFD	= Computational Fluid Dynamic	ρ	= density (kg/m^3)
GTO	= Geostationary Transfer Orbit	T	= Temperature (K)
LEO	= Low Earth Orbit	T_w	= Wall temperature (K)
MECO	= Main Engine Cut Off	u	= Velocity component along the launcher longitudinal axis (m/s)
RLV	= Reusable Launch Vehicle		
SSTO	= Single Stage To Orbit		
TPS	= Thermal protection system		
TSTO	= Two Stage To Orbit		
VTVL	= Vertical Take-off Vertical Landing		

1. Introduction

The European space strategy aims at maintaining autonomous, reliable and cost-effective access to space. Reusability represents a possible approach for reducing costs and improving flexibility of European launch systems. In this framework, the Retro Propulsion Assisted Landing Technologies (RETALT) project, funded by the European Union Horizon 2020 program (grant agreement No 821890) and concluded in the last trimester of 2022, had as objective to study critical technologies for Vertical Takeoff Vertical Landing (VTVL) Reusable Launch Vehicles (RLVs) applying retro propulsion combined with Aerodynamic Control Surfaces (ACS).¹² Two reference launch vehicle configurations, namely RETALT1 and RETALT2, were defined. A comprehensive description of their design and mission concept is provided in Ref.¹²

- RETALT1: A heavy lift Two Stage To Orbit (TSTO) RLV with a payload of up to 14 t into the Geo Transfer Orbit (GTO). The first stage, the only one to be recovered, is powered by nine LOX/LH2 engines inspired to the Ariane's Vulcain 2. The general layout of the RETALT1 configuration is similar to the SpaceX rocket "Falcon 9".

AEROTHERMAL ANALYSIS OF THE RETALT2 VEHICLE

- RETALT2: A smaller Single Stage To Orbit (SSTO) configuration capable to deliver 500kg into Low Earth Orbits (LEO). Despite the similarity to DC-X, RETALT2 is supposed to rely, as well as the other configuration, on European technologies only. The engines are inspired to Vinci engine which uses liquid oxygen and hydrogen (LOX/LH₂), expansion ratios are adjusted to guarantee the optimum thrust. The recovery of the full vehicle is foreseen.

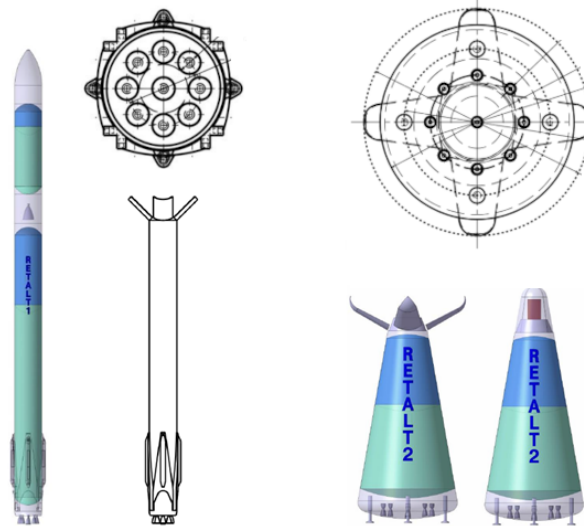


Figure 1: RETALT1 (left) and RETALT2 (right) layout, not to scale.

Since the RETALT2 concept is more novel, its applicability is to be seen more academically compared to RETALT1. The return is performed by exploiting aerodynamic control surfaces together with aerodynamic braking due to its capsule-like shape (e.g. like Soyuz, ExoMars, Hayabusa) which results in a reduction of the overall propellant budget. Retro propulsion is used only for the landing.

Because of this specific re-entry mission profile, the Thermal Protection System (TPS) represents a crucial design element for this configuration. It has to be robust, light-weight, inexpensive and serviceable.¹⁴ The assessment of the instantaneous heat flux at each point of the vehicle and its time integral over the trajectory, that is the thermal load, is of paramount importance in the definition of the TPS material and thickness and for the sizing of other important structural parts like the aerodynamic control surface^{2,13,16} and landing legs.⁸

The evaluation of the thermal loads exerting on the surface of reusable launch vehicles during the flight trajectory is mainly performed via numerical simulations (CFD), in fact extensive experimental campaigns on large-scale vehicles are extremely expensive and wind tunnel tests on lab-scale models are subjected to many limitations. The numerical assessment of the temperature distribution over time requires the coupling of fluid dynamics and material thermo-structural response. Due to the large disparity between the involved time scales, unsteady CFD analysis over the entire trajectory are practically infeasible. To overcome this difficulties a fast-response surrogate model for the aero-thermodynamic heating, called Aero-Thermal DataBase (ATDB), was developed and successfully applied in the framework of RETALT project for predicting the heat flux on each point of the RETALT1 launch vehicle surface as function of flight time and local surface temperature.^{10,11}

The Aero-Thermal DataBase consists of a set of steady-state CFD results for the surface heat fluxes at different trajectory points, operational conditions of the engines and surface temperatures. The assessment of the heat flux on each point of the rocket surface as function of flight time and local surface temperature is made possible by means of interpolation algorithms. The temperature distribution during the overall trajectory can be easily evaluated by coupling the ATDB to a structural response model.

This paper, differently from,^{10,11} describes the creation of Aero-Thermal DataBases for the RETALT2 launch vehicle configuration. One ATDB is generated for the ascent trajectory and a second one for the re-entry flight. Both of them are based on computational matrices which include the most relevant flight regimes, i.e. significant heat fluxes and high dynamic pressure. Furthermore, representative results, obtained from CFD simulations performed for the ATDBs creation, are shown with the aim of discussing typical flow field structures observed during the RETALT2 ascent and entry trajectories and the resulting heating pattern on the rocket surface. In fact, the aero-thermodynamic heating is affected by plume spreading, plume to plume interactions and the presence of hot exhaust gases that surrounds the vehicle during the propelled phases. Aerodynamic forces can also affect the aero-thermodynamic heating.

2. Mathematical & Numerical Model

Steady CFD simulations aimed at solving the Reynolds-Averaged Navier-Stokes (RANS) equations, were performed for the Aero-Thermal DataBases creation. The hybrid structured-unstructured DLR Navier-Stokes solver TAU⁹ was used. The TAU-code is developed by the DLR Institute of Aerodynamics and Flow Technology and is a well established and widely used tool for a broad range of aerodynamic and aero-thermodynamic problems for both scientific and industrial applications. Furthermore the code is adapted for large-scale simulations on massively parallel computers. The TAU code is a second-order finite-volume flow solver for the Euler and Navier-Stokes equations in their integral forms, using eddy viscosity, Reynolds stress, or detached and large eddy simulation for turbulence modeling.

The turbulence model chosen for the present study is the Spalart-Allmaras one-equation eddy viscosity model¹⁵ because of its robustness and capability to reproduce the structure of engine exhaust-plumes during retro-propulsion.^{3-5,16}

The AUSMDV flux-vector splitting scheme combined with MUSCL gradient reconstruction allow to obtain second-order spatial accuracy whilst maintaining a robust numerical treatment of strong discontinuities.

The thermodynamic model used for CFD simulations of RETALT2 ascent flight is based on a mixture of thermally perfect gases. A chemically frozen mixture of air (76 % N_2 and 24 % O_2 by mass fraction) and engine exhaust gas (4.26 % H_2 , 91.33 % H_2O , 3.81 % OH and 0.6 % O_2 by mass fraction) are considered. At the nozzles exit, a constant outflow with temperature of 1708 K, density of 84.39 g/m^3 and Mach number equal to 3.182 is assumed. The properties of the individual species by are either computed from spectroscopic constants using partition functions that include an accurate representation of high temperature effects such as anharmonic-corrections and coupling of rotational and vibrational degrees of freedoms for molecules¹ or from NASA-Polynomials.⁶ Appropriate mixture rules are applied to compute the thermodynamic properties depending on the local gas composition, pressure and density.

The additional heat release due to post-combustion of fuel-rich exhaust gases in the flow field around the rocket is neglected. In fact, in the ascent phase, engine exhaust gases are convected by the flow far away from the surfaces of the vehicle.

Unlike CFD simulations of the RETALT2 ascent trajectory, the thermochemical model used for RETALT2 entry is based on a 5-species non-equilibrium chemical model as described by Gupta et al.⁷ A 5-step reaction mechanism (dissociation of N_2 , O_2 and NO and 2 Zeldovich exchange reactions) from the same reference is used. The choice is motivated by the fact that the Mach numbers during entry are significantly larger than the Mach numbers characterizing the ascent trajectory, moreover, the hypersonic flight regime occurs at high altitude. These conditions are expected to give rise to significant non-equilibrium effects, which the present modeling approach carefully accounts for.

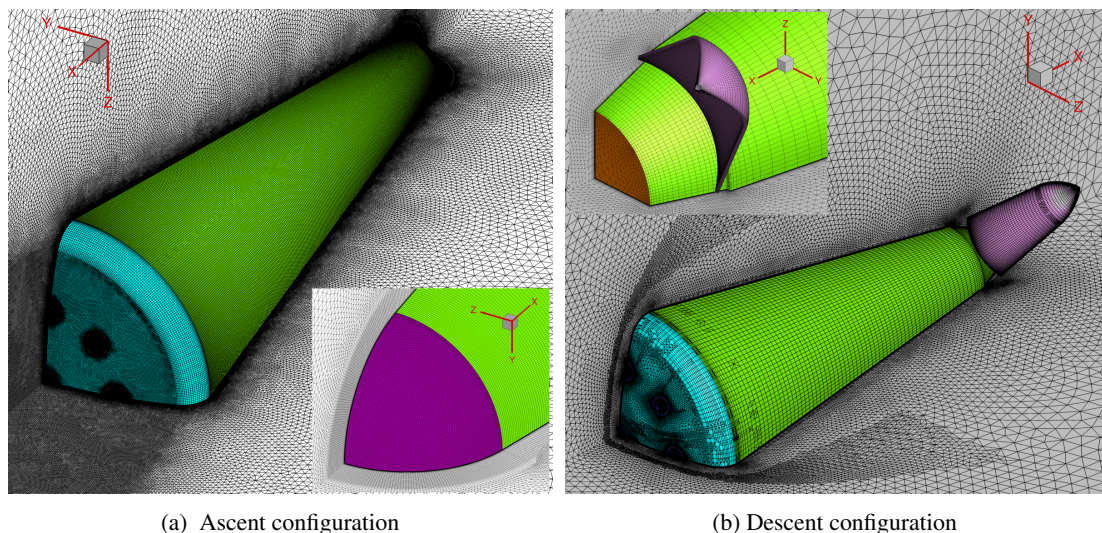


Figure 2: RETALT 2 mesh overview and details.

Regarding mesh generation, TAU uses a cell-vertex finite volume discretization. The unstructured primary grid consists of tetrahedral, prismatic, pyramidal and hexahedral elements.

Wall boundary layers are resolved with prismatic sublayers and a dimensionless first wall distance y^+ close to 1 ensures adequate resolution for the application of the low-Re formulation of the Spalart-Allmaras RANS turbulence model and for accurate heat flux estimation. Assuming an angle of attack of 0 or 180 degrees, CFD simulations can be performed by using a quarter-symmetry model for both the ascent and descent configurations. The hybrid structured/unstructured computational grids include approximately 10M points for the ascent configuration and 1.5M grid points for the descent

AEROTHERMAL ANALYSIS OF THE RETALT2 VEHICLE

configuration. All available geometrical details such as flap hinges are retained in the discretized representation of the vehicle. The grid density is enhanced in regions of particular interest and large flow gradients (e.g. plumes and the near-base recirculation).

3. RETALT2 Mission and CFD data sets

This section provides a description of both the RETALT2 ascent and descent trajectories.

After the ignition of all 9 engines, the launcher lifts off and starts its ascent trajectory. To keep the vehicle's acceleration below 6g, the engines are progressively shut down. After 150.5 s, 5 engines remain active, a phase with 3 active engines follows. Finally only 1 engine remains operational and it is shut down when the vehicle reaches a stable low Earth orbit.

Hereafter, the payload is released and due to the nature of the configuration the aerodynamic control surfaces are deployed at the same time. After that, the vehicle is turned approx. 180° around its pitch axis to fly "backwards". A short retro boost is performed to de-orbit the vehicle. It enters the atmosphere and performs most of the re-entry trajectory aerodynamically, until it is finally decelerated with a landing boost of the central engine until touchdown; while the landing legs are deployed. Finally, the central engine is shut down.

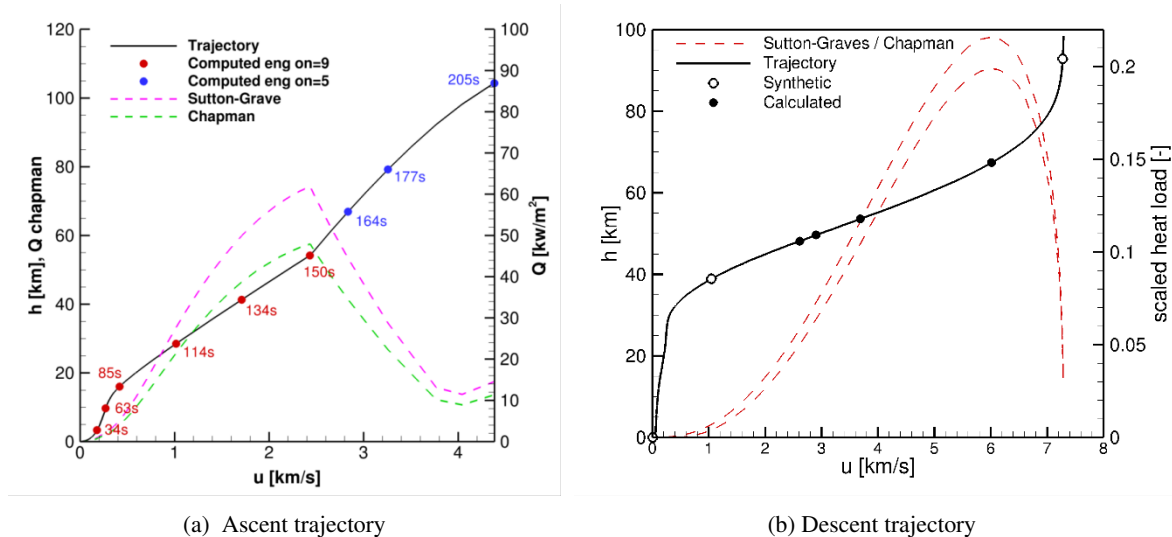


Figure 3: RETALT2 Trajectory points and flight conditions.

The RETALT2 ascent and descent trajectories are shown as solid black lines in Fig.3a and Fig.3b, respectively, along with the heat flux evaluations at the stagnation point obtained using the Chapman and Sutton-Graves approximations (dashed lines).

Regarding the ascent trajectory, the data set contains two significant trajectory points: the maximum Reynolds number, which occurs at 3.3 km, and the maximum heat flux at the stagnation point, which occurs at about 54.2 km. In Fig.3a, solid symbols represent trajectory points for which CFD-analyses were performed. Red symbols indicate the operation of 9 engines whereas the blue ones indicate the operation of 5 engines. For each data point CFD simulations were performed considering 3 fixed wall temperatures: 200 K, 600 K and 1000 K, to account for the influence of the local wall temperature in the aero-thermal database.

The entry flight of the RETALT2, see Fig.3b, is unpropelled, so no plume effects are present. The CFD investigations were performed mainly around the peak heating and critical conditions. Complementary thermal loads at less critical flight conditions (low heating rates) were evaluated using scaling laws and represented by synthetic heat flux distributions (s_1 , s_4 and s_5 in 2).¹⁰ For the generations of the entry flight ATDB only two wall temperatures are considered: 200 K and 600 K. The scaling of the synthetic solutions was also treated separately for all wall temperatures under consideration.

Free stream conditions associated with each data point, number of operative engines and CFD modeling information are listed in Tab.1 and Tab.2 for the ascent and descent configuration respectively.

Table 1: Database population for the RETALT2 ascent configuration

#	Source	time (s)	vel. (km/s)	h (km)	Mach	Nr. Eng. On
1	CFD (turbulent)	33.635	0.179	3.338	0.549	9
2	CFD (turbulent)	62.510	0.271	9.693	0.884	9
3	CFD (turbulent)	85.084	0.418	16.029	1.422	9
4	CFD (turbulent)	114.266	1.017	28.490	3.395	9
5	CFD (turbulent)	134.489	1.711	41.294	5.342	9
6	CFD (turbulent)	150.405	2.433	54.175	7.457	9
7	CFD (turbulent)	164.287	2.835	66.900	9.186	5
8	CFD (turbulent)	177.157	3.258	79.221	11.658	5
9	CFD (turbulent)	205.024	4.384	104.335	14.779	5

Table 2: Database population for the RETALT2 descent configuration

#	Source	time (s)	vel. (km/s)	h (km)	Mach
s1	Scaling from #1	500.68	7.276	92.85	27.38
1	CFD (laminar)	642.94	6.017	67.38	19.57
2	CFD (laminar)	690.20	3.685	53.58	11.29
3	CFD (turbulent)	701.89	2.905	49.65	8.887
4	CFD (turbulent)	706.28	2.613	48.17	8.005
s4	Scaling from #3	735.29	1.048	38.90	3.308
s5	Scaling from #3	1035.1	0.0074	0.00	0.022

4. CFD Representative results

In the next two sub-sections, representative flow field solutions for the RETALT2 ascent and entry trajectories are shown and discussed.

Pictures on the left-side show the surface distribution of the pressure coefficient, the Mach number on the symmetry plane and an iso-surface representing the 50% exhaust mass fraction boundary. This iso-surface indicates the geometrical extend of the plumes. Pictures on the right-side show the heat flux on the vehicle surface, the temperature contour on the symmetry plane and an iso-surface characterized by an axial velocity of -100 m/s, highlighting the presence of recirculation regions.

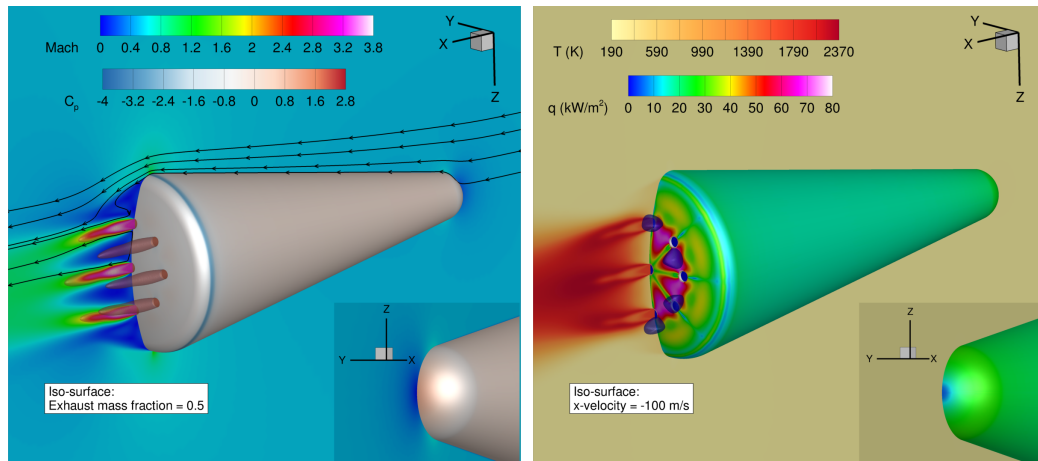
4.0.1 Ascent flight

Relevant flow field phenomena occurring during the ascent flight are described by means of two exemplifying flow field solutions. The first one corresponds to the maximum Reynolds number condition and allows to describe the low altitude mode (see data point #1 in Tab.1 and Fig.4). The second solution instead is related to the maximum heat flux in the stagnation point. It is calculated using Chapman and Sutton-Grave approximations and is representative of the high altitude mode (see data point #6 in Tab.1 and Fig.5).

When the Reynolds number reaches its maximum value the vehicle is immersed in a subsonic flow field. Fig.4a shows that the highest pressure coefficient occurs at the nose tip and slightly decreases moving away from this point. A small increase can be seen in the area connecting the spherical nose to the conical body, then C_p remains approximately constant. Due to the rarefaction wave located at the base plate shoulder the flow becomes supersonic and the pressure coefficient drops down reaching its minimum value. On the base plate C_p is slightly negative. The brown iso-surface allows to notice the presence of nine separated and non-interacting plumes, one for each engine, with a very limited geometric extension. These regions are supersonic.

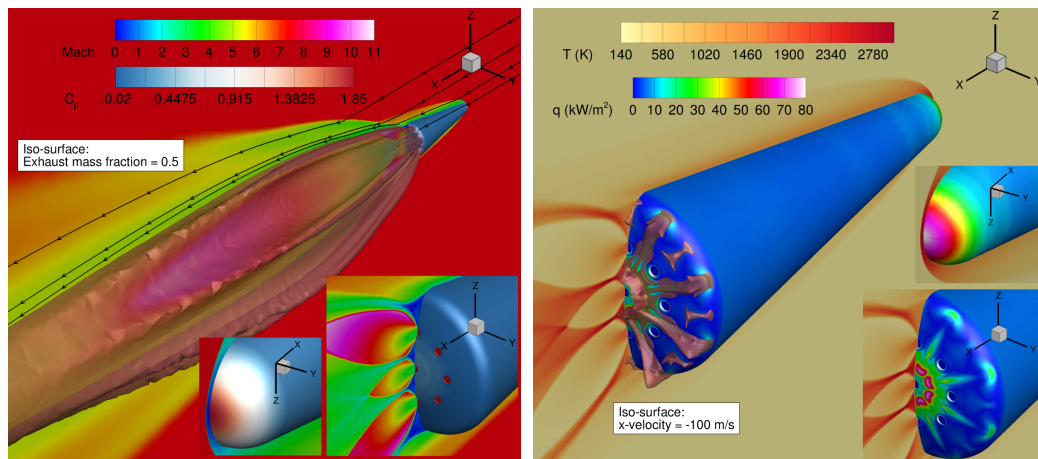
Fig.4b highlights that the highest temperatures occur in the plume regions. The streamlines show that the flow is aligned to the vehicle surface and therefore the heat flux remains rather low. The blue iso-surface registers the presence of low-level recirculation at the base plate, in particular the back flow is limited to small "pockets" between the lateral engines. It is very interesting to note that the heat flux pattern on the base plate is strongly related to the back flow trace.

AEROTHERMAL ANALYSIS OF THE RETALT2 VEHICLE



(a) Pressure coefficient (surface), Mach number (symmetry plane), 50% exhaust gases mass fraction (iso-surface).
 (b) Heat flux (surface), Temperature (symmetry plane), x -velocity=-100 m/s (iso-surface).

Figure 4: RETALT2 flow field at max Re conditions (flow conditions #1 in Tab.1).



(a) Pressure coefficient (surface), Mach number (symmetry plane), 50% exhaust gases mass fraction (iso-surface).
 (b) Heat flux (surface), Temperature (symmetry plane), x -velocity=-100 m/s (iso-surface).

Figure 5: RETALT2 flow field at max stagnation heat flux conditions (flow conditions #6 in Tab.1).

At higher altitudes the reduction of ambient pressure and density causes a significant plume spreading and plume to plume interaction phenomena, as can be evinced by looking at Fig.5a. Differently from the previous case the brown iso-surface, which describes the plume extent, shows a strong interaction of the engine plumes and an enlargement of the region characterized by 50% exhaust mass fraction mainly in the axial direction but also in the radial one.

The flow field solution discussed in Fig.5 is supersonic. Because of the bow shock located in front of the vehicle the pressure coefficient exhibits its maximum value of the nose tip and decreases moving downstream. C_p is slightly negative on the vehicle body and also on the base plate.

High temperatures are detected at the stagnation point and in the plume region as shown in Fig.5b. With regard to the heat fluxes the presence of the bow shock is also the cause of the strong heating of the nose tip. According to the Chapman and Sutton-Grave approximations, the maximum value of the heat flux at the stagnation point for the ascent trajectory occurs precisely with these free stream conditions. On the vehicle body, due to the moderate densities and flow direction, which is essentially aligned to the surface, the heat flux remains moderate.

The recirculation region exhibits a different pattern compared to the low-altitude case, in fact here is located around the central nozzle and in the radial directions corresponding to the outer nozzles, additional small pockets can be found on the base plate shoulder. The heat flux pattern once again is correlated to the presence of the back flow that pushes the hot and low-speed gases onto the vehicle surface enhancing the heat exchange.

4.0.2 Entry flight

Representative flow field solutions for the unpropelled RETALT2 configuration at Mach numbers of 20 and 8 during atmospheric entry are shown in Fig.6a and Fig.6b respectively. The distributions of surface heat flux and Mach number across the symmetry plane are shown in different color scales. The blue line represents the sonic line. The dark-gray iso-surface depicts zones of flow reversal (separation zones upstream of the control surfaces). Significant heat loads occur at the front and at the control surfaces of the vehicle. Small surface distortions around the flush-mounted thrust nozzles generate strong local amplification of surface heat flux (radial streaks in Fig.6a). A large zone of flow separation develops upstream of the control surfaces. The size of this zone decreases at lower altitudes which is mainly due to laminar to turbulent transition and the associated larger resistance to separation of turbulent boundary layers. Flow separation affects the aerodynamic efficiency of the control surfaces and causes significant local heat loads at the reattachment point.

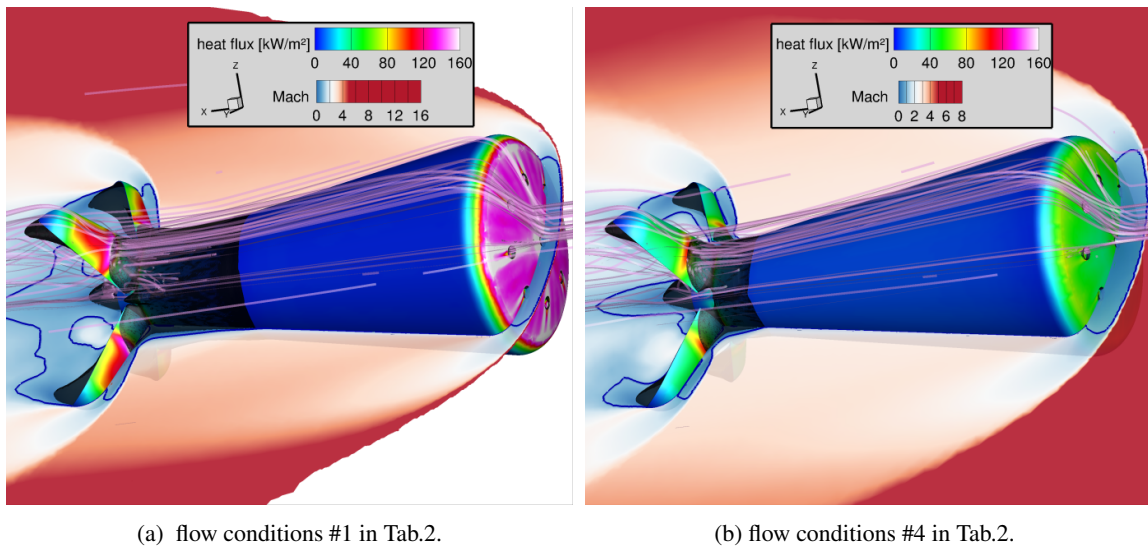


Figure 6: RETALT2 flow fields during re-entry flight.

5. Heat loads

This section describes the heat flux distributions at constant wall temperatures for the atmospheric ascent and descent of the RETALT2 vehicle. Results represent convective heating only at constant wall temperatures of 200 K and 600 K, without radiation effects or structural response. They are intended to provide an estimate of external heat load distributions for the evaluation and design of TPS systems.

5.0.1 Ascent flight

The time evolution of area-averaged heat fluxes on the vehicle nose (red lines) and base plate (blue lines) for constant wall temperatures are shown in Fig.7.

The nose heating at relatively low flight velocities ($t < 110$ s, Mach 3.5) is dominated by the difference of the wall and ambient temperature (heating for $T_w < T_{ambient}$, cooling for $T_w > T_{ambient}$). At a flight time approximately equal to 85 s it is possible to observe a slope change due to the subsonic-supersonic transition. In the time range 110 – 160 s the nose experiences high heat fluxes, see also Fig.8b. The nose heating curves collapse at $t = 160$ s because the total temperature is significantly larger than the wall temperature.

Concerning the base plate, it is interesting to observe that in the time range between the lift off and $t < 110$ s, the time evolution of the area-averaged heat flux is also ruled by the difference of the wall and ambient temperature (heating for $T_w < T_{ambient}$, cooling for $T_w > T_{ambient}$). In fact the flow topology related to the low-altitude mode is characterized by limited plume to plume interactions, so that large areas of the base plate, in particular the outer region, are not affected by engine plumes. see Fig.8a.

For $t > 110$ s the area-averaged heat flux remains essentially constant. In the high-altitude mode the size of the plume is significantly larger due to the ambient pressure and density reduction leading to an intensification of plume to plume

AEROTHERMAL ANALYSIS OF THE RETALT2 VEHICLE

interactions which gives rise to strong local recirculation patterns. In fig.8c the different heat flux pattern is due the operation of 5 engines instead of 9.

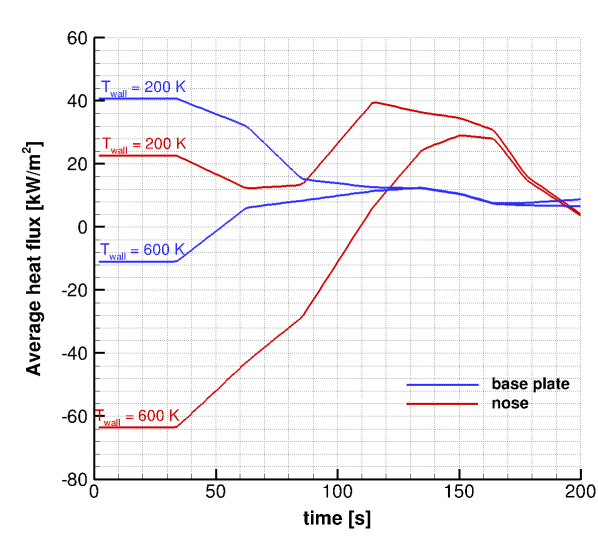


Figure 7: Time evolution of RETALT2 average heat fluxes for constant wall temperatures (ascent).

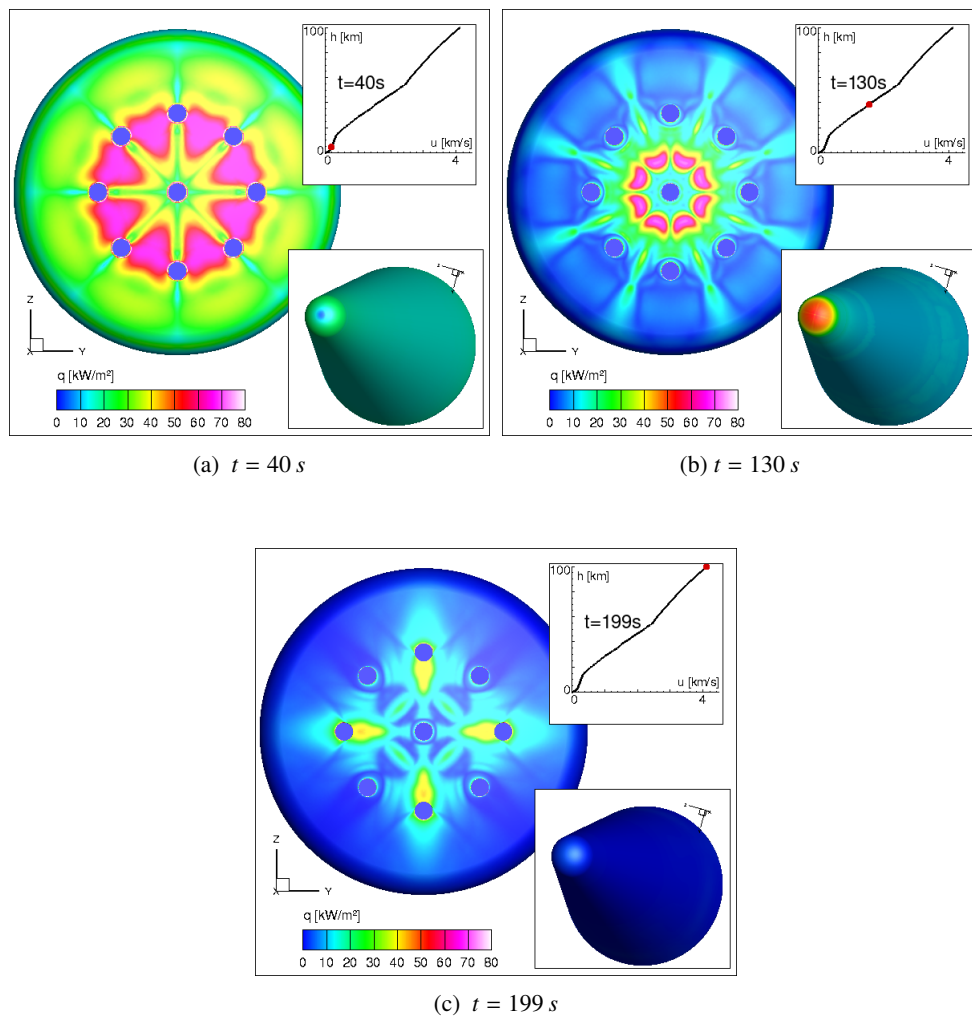


Figure 8: RETALT2 ascent heat flux distributions at different flight times ($T_w = 200 K$).

5.0.2 Entry flight

The time evolution of area-averaged heat fluxes on the RETALT2 vehicle, during the re-entry trajectory, is shown in Fig.9. Solid and dashed lines correspond to constant wall temperatures of 200 K and 600 K, respectively.

Results in Fig.9 show that a significant heating occurs during a period of flight time between 500 and 740s. The prolonged exposure to high heat fluxes results in significant heat loads, which, by definition, are calculated as the time integral of the heat fluxes.

Concerning fins (aerodynamic control surfaces), heat fluxes shown in Fig.9 represent the average of the windward and the leeward side. Due to the negligible heat fluxes at the leeward side, the average on the windward side only is approximately twice the value of the entire fin.

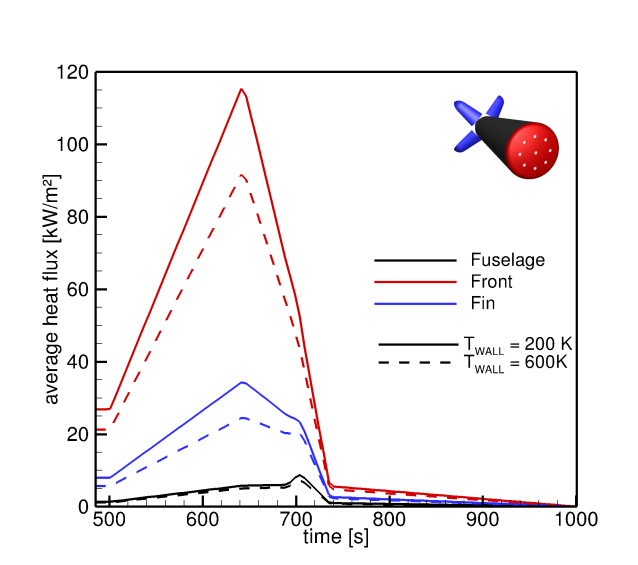
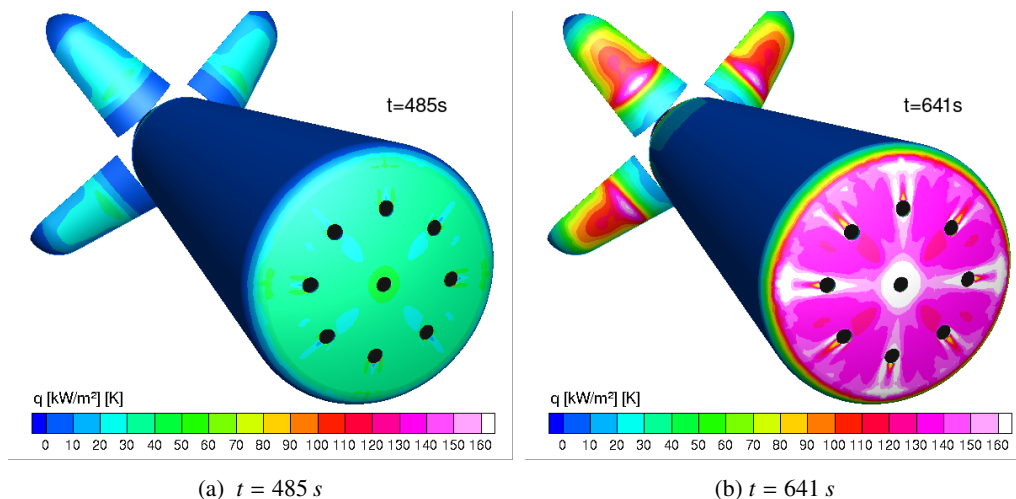


Figure 9: Time evolution of RETALT2 average heat fluxes for constant wall temperatures (descent).

Results in Fig.9 allow also to evaluate the impact of the wall temperature on the heat fluxes. Assuming $T_w = 600\text{ K}$, heat fluxes decrease by less than 30% compared to the cold wall assumption ($T_w = 200\text{ K}$).

Representative heat flux distributions for a constant wall temperature of 200K are shown in Fig.10. The qualitative heat flux distribution is not affected by the wall temperature, therefore the heat flux pattern for hot walls can be approximately obtained by scaling down the contours by the factor shown in Fig.9.

The heat flux distribution on the front heat shield is nearly homogeneous with hot streaks caused by the surface disturbances of the nozzles exit. The control surfaces are exposed to strongly non-uniform heating with a distinct peak at the flow re-attachment zone (see Fig.6 for the flow topology).



(a) $t = 485\text{ s}$

(b) $t = 641\text{ s}$

AEROTHERMAL ANALYSIS OF THE RETALT2 VEHICLE

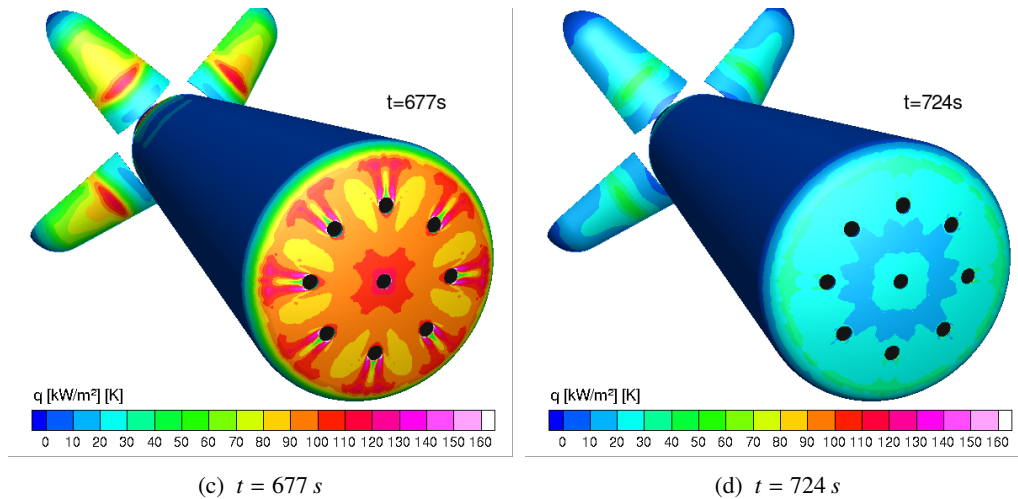


Figure 10: RETALT2 descent heat flux distributions at different flight times $T_w = 200$ K.

6. Conclusions

In the framework of the Horizon 2020 project RETALT (Retro Propulsion Assisted Landing Technologies), the thermal loads exerting on the surface of RETALT2 configuration, during its entire flight trajectory, were evaluated. The assessment of thermal loads is essential for the design of the thermal protection system which is a crucial design element for this configuration due to its peculiar re-entry mission profile.

A fast response surrogate model for aero-thermodynamic heating was created. This model is based on an aerothermal database (ATDB) consisting of a large set of steady-state CFD results for the surface heat fluxes for different trajectory points, engine operating conditions, and surface temperatures. Interpolation algorithms allow the heat flux estimation at any point on the launcher surface as a function of flight time and local surface temperature. In addition, the ATDB can be easily coupled with a structural response model to obtain the temperature distribution on the launcher surface over time.

The computational matrix covers both the RETALT2 ascent and entry trajectory. Steady RANS simulations were performed mainly around peak heating and at critical flight conditions exploiting the hybrid structured-unstructured DLR Navier-Stokes solver TAU, whereas scaling laws were used to evaluate thermal loads in aerodynamic flight conditions characterized by low heating rates.

The paper is focused on the flow topology analysis of representative solutions obtained during the RETALT2 ascent and entry trajectory. The time evolution of area-averaged heat fluxes on different parts of the vehicle are also discussed.

Concerning the ascent, two flow modes are observed. At low altitude engine plumes are confined and plume to plume interactions are limited, the heating on the base plate is driven by the difference of the wall and ambient temperature. The same mechanism dominates also the nose heating. At higher altitudes, due to the lower ambient pressure and density, plumes spread significantly behind the launch vehicle. This leads to an intensification of plume to plume interaction phenomena which give rise to strong local recirculation patterns. The heat flux footprint on the base plate is closely connected to the presence of the back flow that pushes hot and low-speed gases onto the vehicle surface enhancing the heat exchange.

The entry flight of the RETALT2 is unpropelled, so no plume effects are present. At high altitude the front part of the vehicle and the control surfaces experience significant heat loads. A large zone of flow separation develops upstream of the control surfaces. The size of this zone decreases at lower altitudes which is mainly due to laminar to turbulent transition and the associated larger resistance to separation of turbulent boundary layers. Flow separation affects the aerodynamic efficiency of the control surfaces and causes significant local heat loads at the reattachment point.

In conclusion it is possible to state that the Aero-Thermal Database represents a valuable tool for the preliminary evaluation of the thermal loads occurring on the launcher surface and the identification of critical flow conditions.

7. Acknowledgments

This project has received funding from the European Union's Horizon 2020 research and innovation framework program under grant agreement No 821890. We gratefully acknowledge the interest in our work and the opportunity to forward this essential research.

References

- [1] B. Bottin. Aerothermodynamic model of an inductively-coupled plasma wind tunnel. *PhD-Thesis, University of Liege*, 1999.
- [2] D. Charbonnier, J. Vos, A. Marwege, and C. Hantz. Computational fluid dynamics investigations of aerodynamic control surfaces of a vertical landing configurations. *CEAS Space Journal*, doi:10.1007/s12567-022-00431-6, 2022.
- [3] T. Ecker, S. Karl, E. Dumont, S. Stappert, and D. Krause. Numerical study on the thermal loads during a supersonic rocket retropropulsion maneuver. *Journal of Spacecraft and Rockets* 57(1) 131-146, 2020.
- [4] Tobias Ecker, Moritz Ertl, Joseph Klevanski, Etienne Dumont, and Sven Krummen. Aerothermal characterization of the callisto vehicle during descent. In *9th European Conference for Aeronautics and Space Sciences*, 2022.
- [5] M. Ertl, T. Ecker, J. Klevanski, S. Krummen, and E. Dumont. Aerothermal analysis of plume interaction with deployed landing legs of the CALLISTO vehicle. *9th European Conference for Aeronautics and Space Sciences*, 2022.
- [6] S. Gordon and B. J. McBride. Computer program for calculation of complex chemical equilibrium compositions and applications. *NASA Reference Publication 1311*, 1994.
- [7] R.N. Gupta, J.M. Yos, R.A. Thompson, and K.P. Lee. A review of reaction rates and thermodynamic and transport properties for an 11-species air model for chemical and thermal nonequilibrium calculations to 30000 k. *NASA Reference Publication, No. 1232*, 1990.
- [8] A. Krammer, L. Blecha, and M. Lichtenberger. Fin actuation, thrust vector control and landing leg mechanisms design for the retalt vtvl launcher. *CEAS Space Journal*, <https://doi.org/10.1007/s12567-021-00421-0>, 2022.
- [9] S. Langer, S. Schwöppe, and N. Kroll. The dlr flow solver tau-status and recent algorithmic developments. *AIAA Paper 2014-0080*, 2014.
- [10] M. Laureti and S. Karl. Aerothermal databases and load predictions for retro propulsion assisted launch vehicles (retalt). *CEAS Space Journal*, <https://doi.org/10.1007/s12567-021-00413-0>, 2022.
- [11] M. Laureti, S. Karl, A. Marwege, and A. Gülhan. Aerothermal Databases and CFD Based Load Predictions. *2nd International Conference on Flight Vehicles, Aerothermodynamics and Re-entry Missions and Engineering (FAR)*, Heilbronn, Germany, Jun 2022, <https://doi.org/10.5281/zenodo.6759561>.
- [12] A. Marwege, A. Gülhan, J. Klevanski, C. Hantz, S. Karl, M. Laureti, G. De Zaiacomo, J. Vos, M. Jevons, C. Thies, A. Krammer, M. Lichtenberger, J. Carvalho, and S. Paixão. RETALT: review of technologies and overview of design changes. *CEAS Space Journal*, Jun 2022, <https://doi.org/10.1007/s12567-022-00458-9>.
- [13] A. Marwege, C. Hantz, D. Kirchheck, J. Klevanski, A. Gülhan, D. Charbonnier, and J. Vos. Wind tunnel experiments of interstage segments used for aerodynamic control of retro-propulsion assisted landing vehicles. *CEAS Space Journal*, <https://doi.org/10.1007/s12567-022-00425-4>, 2022.
- [14] S. Paixão, C. Peixoto, M. Reinas, and J. Carvalho. Retalt tps design and manufacturing. *CEAS Space Journal*, <https://doi.org/10.1007/s12567-021-00417-w>, 2022.
- [15] P.R Spalart and S.R Allmaras. A one-equation turbulence model for aerodynamic flows. *AIAA Paper 1992-0439*, 1992.
- [16] J. Vos, D. Charbonnier, A. Marwege, A. Gülhan, M. Laureti, and S. Karl. Aerodynamic investigations of a vertical landing launcher configuration by means of computational fluid dynamics and wind tunnel tests. *AIAA SCITECH 2022 Forum*, <https://doi.org/10.2514/6.2022-1308>, San Diego, 2022.